RF Project 762100/712767
Final Report

the ohio state university
research foundation
1314 kinnear road
columbus, ohio
43212

INTEGRATED FLUXES FOR EMISSION LINES IN THE ULTRAVIOLET SPECTRA OF SEVERAL PLANETARIES

Kenneth G. Carpenter and Stanley J. Czyzak
Department of Astronomy

For the Period
April 15, 1980 - June 30, 1981

NATIONAL AERONAUTICS AND SPACE ADMINISTRATION
Goddard Space Flight Center
Greenbelt, Maryland 20771

Grant No. NAG 5-42

November, 1981

Integrated Fluxes for Emission Lines in the Ultraviolet Spectra of Several Planetaries

Kenneth G. Carpenter and S. J. Czyzak
Department of Astronomy
The Ohio State University
Columbus, Ohio 43210

Abstract

The IUE satellite observatory has been used to obtain absolutely-calibrated emission line fluxes for diagnostic lines of multiply-ionized C, N, O, Si, Ne, and Ar which occur in the ultraviolet spectral region of planetary nebulae. These data, when combined with data from the blue, visual, and near infrared, will provide improved estimates of ionic concentrations, plasma temperatures and densities, and elemental abundances.

I. Introduction

The IUE satellite has made it possible to study diagnostic lines in the ultraviolet spectral region of nebulae. Since a number of ions have their strongest lines in the ultraviolet region observable with the IUE (1150 - 3200A), a large number of lines important in nebular calculations can be studied with this satellite. These include the following lines: C III] (λ 1906, 1909), C IV (λ 1548, 1550), N III] (λ 1750), N IV] (λ 1487), N V (λ 1243), O III] (λ 1661, 1666), O IV (λ 1403, 1409), O V (λ 1371), Si III (λ 1892), Ne IV (λ 2423, 2425), and Ar IV (λ 2854).

Recent work on a number of nebulae in the blue and visual regions (Aller and Czyzak, 1979) suggests that an examination of the ultraviolet spectral region of these nebulae is desirable. Also, newer, more accurate ultraviolet transition probabilities are now available for oxygen and nitrogen ions (Czyzak and Krueger, 1979).

We have observed the following six nebulae: J-900, IC 2165, IC 4997, NGC 2022, NGC 6572, and NGC 7009. The IUE satellite was used in order to obtain integrated line fluxes for as many of the diagnostic lines as possible. The observations obtained and the reduction methods employed to calculate the line fluxes are detailed in the following section.

II. Observations and Data Reduction

A. Observations

Low dispersion spectrograms (resolution $\sim$ 6 A) of all six nebulae were obtained with both the SWP (short-wavelength prime) and LWR (long-wavelength redundant) cameras through the large (10 x 20 arcsec oval) entrance aperture. The SWP camera records the 1150 - 2000 A region and the LWR camera records the 1700 - 3400 A region, although the later is not very sensitive below about 1900 A.

Three of the nebula (IC 4997, NGC 6572, NGC 7009) were also observed in both wavelength regions in the high dispersion echelle mode (resolution about 0.2 A). Again, the large entrance aperture was used for all exposures. The design and in-flight performance of IUE is described by Boggess et al. (1978a, 1978b). These data are summarized in Table I which gives for each exposure the image number, name of the object, dispersion mode, exposure time, and the date the image was taken.

A sample of these data are plotted in figures 1-3. Figures 1 and 2 show the low dispersion spectra of NGC 6572 and IC 2165 for both spectral regions. Note in NGC 6572 the strong stellar continuum and the clear P-Cygni profiles of the Ly$_\alpha$ λ 1215, N V λ1243, O V λ1371, and C IV λ1549 lines.

Aside from the same N V and O V lines in NGC 7009, no other P - Cygni profiles are seen in any of the exposures;

the other spectra look much the same as IC 2165, although relative line strengths do vary from object to object. Figure 3 shows a sample of the high resolution data for NGC 7009. The ratio of the strength of these two lines in the C III doublet near 1908 A is sensitive to electron density (Nussbaumer and Schild, 1979). Since they also happen to be among the strongest lines visible in IUE spectra of planetary nebula, they are thus a valuable diagnostic aid. However, their strength can also be a disadvantage; on spectra deep enough to show a decent number of other lines, these C III lines are frequently overexposed (as in our NGC 6572 spectrum). We also note that the apparent feature to the blue side of the λ 1906 line is spurious, caused by the proximity of the end of order 72 on this high dispersion echellogram.

B. Data Reduction

The basic low resolution data were the absolutely-calibrated, time-integrated spectra provided by the IUE observatory on the Guest Observer's magnetic tape (the "eslo" files). Flux values were computed every .25 A, by linear interpolation in the original data, to allow more precision in choosing the wavelength limits for each line integration. The trapezoid rule was used to perform the integrations. The resulting numbers were then divided by the exposure time to obtain absolute fluxes in ergs-cm^{-2} -sec^{-1} at the earth.

The reduction of the high resolution data is less straightforward since a standard absolute calibration has not yet been adopted by the IUE observatory for high resolution images. In order to present the results on a scale other than the straight instrumental one, we have elected to use the preliminary high dispersion calibration of Cassatella et al. (1981). These authors define a factor $C_\lambda = n_\lambda / N_\lambda$, the ratio, at a given wavelength, of the slit-integrated net IUE Flux Numbers /sec from low resolution spectra (n_λ) to similarly derived numbers (N_λ) from high resolution spectra. Thus $C_\lambda S_\lambda^{-1}$, where S_λ^{-1} is the inverse sensitivity function for IUE low resolution spectra, is the inverse sensitivity function for high resolution spectra. Hence the absolute flux (erg/cm^2/sec/A) $= n_\lambda S_\lambda^{-1}$ for low resolution data and $= N_\lambda C_\lambda S_\lambda^{-1}$ for high resolution data. C_λ was determined from comparisons of pairs of low and high dispersion spectra of the same object, after the resolution of the high dispersion data had been degraded to that of the low dispersion data. C_λ was obtained for both cameras for all wavelengths for continuous sources but C_λ could be defined properly for emission-line spectra only in restricted spectral regions for each camera, due to a lack of good quality data outside of these regions. Their equations (7) ($C_\lambda = 228.009 - 0.0755\lambda$) and (8) ($C = 167.099 - 0.0229\lambda$) are valid for emission line spectra in the 1400 - 1975 A region of the SWP camera and the 2300 - 3100 A region of the LWR camera, respectively. The net

ripple-corrected spectra ("eshi" files on the Guest Observer tape) were the basic data for the high resolution analysis. As in the low-resolution reductions, linear interpolation was used to define the spectra on a finer wavelength grid ($\Delta\lambda$ = .01 A in this case) and the trapezoid rule was used to perform the integrations. These numbers were then divided by the exposure time and multiplied by the $C_\lambda S_\lambda^{-1}$ listed in Table III. The $C_\lambda S_\lambda^{-1}$ are listed in that table to allow the reader to account for any changes which may be made in the high-resolution calibration factors assumed here.

III. Results and Discussion

The integrated line fluxes for the low and high resolution spectra along with the proposed identifications of each feature are presented in Tables II and III, respectively.

The data presented in Table II for low resolution spectra should be quite reliable. With the high signal/noise ratio in all these low resolution spectra, good flux measurements were obtained. The ease of the feature identification process and the reasonableness of the identifications given indicate a low probability that any of these are spurious.

The situation for the high resolution data is not quite as satisfactory. All these spectra are fairly long exposures with a low signal/noise ratio over large fractions of the spectral range. We have tried to insure that only real lines

were measured and listed in the table of fluxes, but the reader should be aware that some of the features measured, in particular the weaker unidentified features, may not be real. Unless a question mark appears in the ID column we feel the identifications given are reliable. We have noted in both tables where either partial detector saturation or the proximity of reseau marks limits the accuracy of the flux measurements.

The combination of the flux measurements with data from other wavelength regimes will provide an opportunity to improve estimates of ionic concentrations, plasma temperature and densities, and elemental abundances in each of these planetary nebulae.

Acknowledgements

This work was supported in part by NASA Grant NAG 5-42 to The Ohio State University. We thank Dr. A. Boggess and the staff of the IUE Observatory for their assistance in the acquisition and reduction of these data. To Dr. L. H. Aller we are grateful for his suggestions and comments.

References

Aller, L. A. and Czyzak, S. J. 1979, Astrophy. and Sp. Sci. 62, 397.

Boggess, A. et al. 1978a, Nature, 275, 372.

_____. 1978b, Nature, 275, 377.

Cassatella, A., Ponz, D. and Selvelli, P. L. 1981, IUE Newsletter No. 14.

Czyzak, S. J. and Krueger, T. K. 1979, Astrophys. and Sp. Sci. 60, 99.

Nussbaumer, H. and Schild, H. 1979, Astron. Astrophys. 75, L 17.

Table I

Summary of Exposures

	Image #	Object	Dispersion	Exp. Time	Date Taken
SWP	8667	IC 4997	L	5 min.	Apr. 5, 1980
	8668	IC 4997	H	120	"
	8669	NGC 6572	L	15	"
	8670	NGC 6572	H	120	"
	8676	NGC 2022	L	45	Apr. 6, 1980
	8677	J-900	L	30	"
	8678	IC 2165	L	20	"
	8679	NGC 7009	L	4	"
	8680	NGC 7009	H	20	"
LWR	7419	IC 4997	L	20	Apr. 5, 1980
	7420	IC 4997	H	180	"
	7421	NGC 6572	L	12	"
	7422	NGC 6572	H	120	"
	7424	NGC 7009	H	60	"
	7428	NGC 2022	L	60	Apr. 6, 1980
	7429	J-900	L	45	"
	7430	IC 2165	L	30	"
	7431	NGC 7009	L	8	"

Table II

Integrated Line Fluxes from Low Resolution Spectra
(units = 1 x 10^{-12} ergs/cm^2/sec)

Obs. λ	Lab. λ	ID	IC4997	N6572	N2022	J-900	IC2165	N7009
		SWP spectra						
1242	1243	N V		3.89[2]				25.2[2]
1373	1371	O V		1.14[2]				6.21[2]
1399	1406	O IV			1.07[r]		.992	
1486	1486	N IV]		1.93[1]	.848		.720	
1543	1549	C IV	2.64	5.19[2]	10.9	5.39	22.7	6.33
1638	1640	He II		2.57	9.78	1.62	6.79	41.7
1662	1663	O III]	4.07[r]	2.36[r]				2.86[r]
1719				1.11				
1751	1750	N III]	3.37	3.01			.791	6.25
1904	1909	C III]	17.6	50.0[s]	5.37	8.78[s]	22.8	23.0
		LWR spectra						
1915	1909	C III]	19.8	50.4	6.72	8.33	21.8	31.5
2255	2253	He II	.566			.507		
2301	2297	C III?						4.58
2330	2321	[O III]	2.16	13.0		1.14	1.54	
	2323	C II]						
2426	2424	[Ne IV]			3.72	.604	2.50	2.88
2474	2470	[O II]	1.70	6.11				

Table II (continued)

Integrated Line Fluxes from Low Resolution Spectra
(units = 1 x 10^{-12} ergs/cm^2/sec)

Obs. λ	Lab. λ	ID	IC4997	N6572	N2022	J-900	IC2165	N7009
			LWR spectra					
2735	2733	He II			.578		.594	1.46
2801	2796	Mg II	2.18^s					
	2803	Mg II						
2839	2836	O IV		1.49		.179	.397	3.31
2948				.743				
3027	3023	O III						2.13
3050	3047	O III					.800	6.54
3137	3133	O III		1.25	2.18	2.07	6.11	30.8

s = contains saturated pixel.

r = contaminated by reseau.

1. Broad, noisy feature unlike any other in this spectrum.

2. Measure of emission component of strong P-Cygni profile.

Note: Lyα is not measured because of the strong geocoronal contamination.

Table III
Integrated Line Fluxes from High Resolution Spectra
(units = 1 x 10^{-12} ergs/cm^2/sec)

Obs. λ	Lab. λ	ID	N6572	IC4997	N7009	$C_\lambda S_\lambda^{-1}$
1413.52				.953		3.29
1444.32				.461		3.54
1533.94				.491		4.23
1537.03				.509		4.24
1547.93	1548.2	C IV	1.08	1.75	3.14	4.26
1549.62					2.35	4.26
1550.42	1550.77	C IV	1.44	1.50	2.04	4.26
1583.81				.756[r]		3.94
1590.42			.978			3.87
1639.73				.814		3.34
1640.84	1640.33	He II		.439	41.6	3.33
1660.40	1660.80	O III]	1.03	1.55		3.13
1663.37				.331		3.10
1665.73	1666.15	O III]	2.03	3.76	1.74	3.06
1718.37				.184		2.55
1748.06	1748.61	N III]	.471	.280		2.28
1749.21	1749.67	N III]	1.39	1.21	1.53	2.27
1751.61	1752.16	N III]	.882	.635		2.24
1757.47				.296		2.21
1795.51			.375	.258	.695	1.95
1796.43			.301	.349		1.95
1810.27				.270		1.90
1814.22				.257		1.89
1882.55			.332[RQ]			1.75

Table III (continued)
Integrated Line Fluxes from High Resolution Spectra

Obs. λ	Lab. λ	ID	N6572	IC4997	N7009	$C_\lambda S_\lambda^{-1}$
1884.00			.192	.312[RQ]		1.75
1888.61			.726			1.74
1891.53	1892.03	Si III	.392	.428		1.73
1906.30	1906.68	C III]	23.9[s]	1.25	18.6	1.71
1908.43	1908.73	C III]	23.9[s]	20.3[s]	12.2	1.70
2320.31	2320.95	[O III]	.649	.703		1.06
2323.55	2323.50	C II]	1.46			1.04
2324.44	2324.69	C II]	.762			1.04
2325.28	2325.40	C II]	4.29	.653		1.04
2326.29	2326.93	C II]	2.58	.334		1.03
2327.93	2328.12	C II]	.684			1.02
2421.28	2421.65	N IV			1.34	.723
	2422.60	[Ne IV]				
2423.91	2425.24	[Ne IV]			1.45	.715
2469.75	2470.30	[O II]	5.52[s]	1.52		.608
2510.73	2511.21	He II			1.34	.537
2517.43				.121[r]		.529
2655.22					.367	.387
2663.10			.158			.381
2691.58					.218	.362
2695.91			.257			.360
2722.99			.365			.351
2732.77	2733.30	He II			1.82	.348

Table III (continued)
Integrated Line Fluxes from High Resolution Spectra

Obs. λ	Lab. λ	ID	N6572	IC4997	N7009	$C_\lambda S_\lambda^{-1}$
2745.20					.316	.345
2759.44				.086		.343
2763.20			.387	.115		.343
2775.75				.172[RQ]		.341
2785.04				.075		.341
2793.08			.091	.059		.340
2794.73	2795.52	Mg II	.198	.130		.339
2795.98			.314			.339
2801.96	2802.70	Mg II	.126	.930		.339
2803.10			.215			.339
2807.84			.286			.340
2811.12				.137		.340
2828.63	2829.16	O IV?	.547	.225	.674	.342
2835.79	2836.26	O IV			3.32	.343
2853.13	2853.64	[Ar IV]	.252	.345	.511	.345
2858.75	2859.16	N V?		.463		.348
2900.80				.177	.302	.369
2921.22	2921.45	O IV?		.074		.386
2942.08				.123		.403
2944.69			1.52		.775	.406
2972.19	2972.56	N III?		.102		.439
2980.64				.132		.451
3010.79				.097		.500

Table III (continued)
Integrated Line Fluxes from High Resolution Spectra

Obs. λ	Lab. λ	ID	N6572	IC4997	N7009	$C_\lambda S_\lambda^{-1}$
3022.91	3023.45	O III			1.25	.527
3024.47				.152		.540
3046.69	3047.13	O III			3.23[r]	.580
3066.77				.329		.666
3132.37	3132.86	O III			22.5[r]	1.08[1]
3202.50	3203.10	He II			5.75	2.03[1]

r = reseau

RQ = reality questionable

1 Accuracy of calibration uncertain at these wavelengths.

Notes:

1. Features shortward of 1400 Å are not included in this table since the absolute-calibration is not defined at those wavelengths for high resolution emission-line spectra.

2. Data from lines below 2000 A are from the SWP camera while data from lines above 2000 A are from the LWR camera.

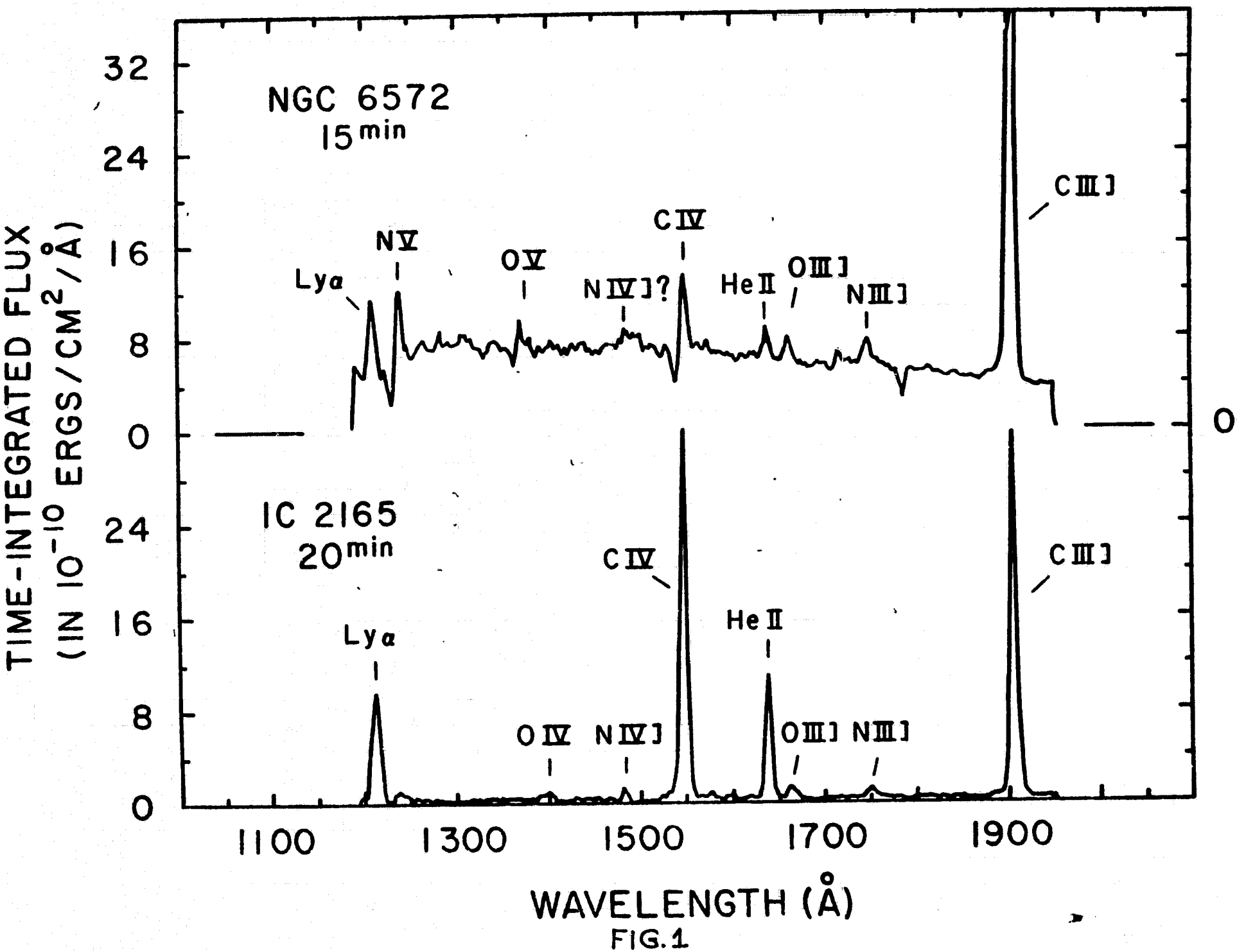
NGC 6572
15 min
IC 2165
20 min
Lyα
NV
OV
NIV]?
CIV
HeII
OIII]
NIII]
CIII]
OIV
0
8
16
24
32
1100
1300
1500
1700
1900
TIME-INTEGRATED FLUX
(IN 10^{-10} ERGS/CM^2/Å)
WAVELENGTH (Å)

FIG.1

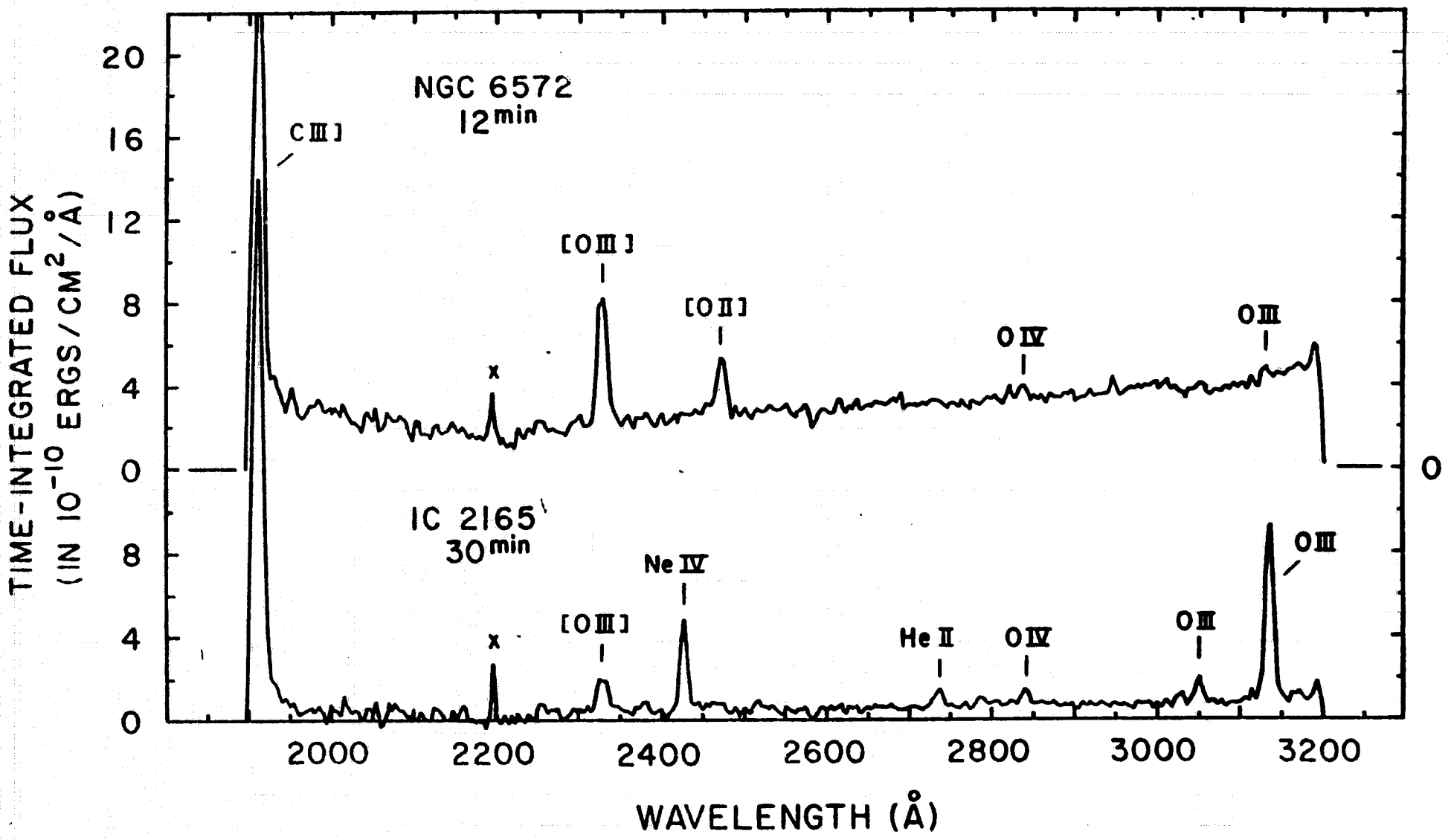
NGC 6572
12min
C III]
[O III]
[O II]
O IV
O III
x
IC 2165
30min
Ne IV
[O III]
He II
O IV
O III
O III
x
TIME-INTEGRATED FLUX
(IN 10^{-10} ERGS/CM^2/Å)
WAVELENGTH (Å)
20
16
12
8
4
0
8
4
0
2000
2200
2400
2600
2800
3000
3200

FIG 2

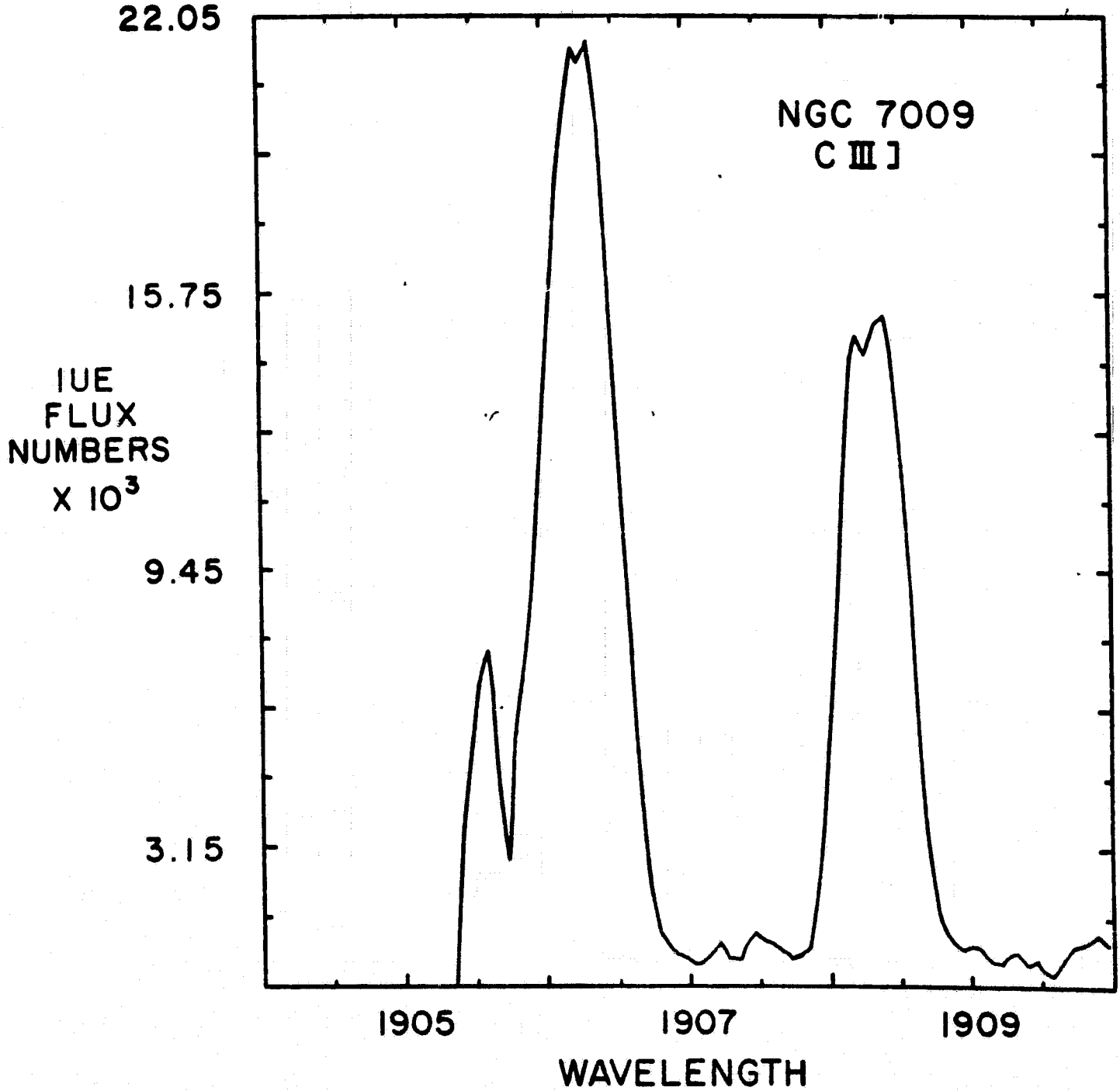
22.05
15.75
9.45
3.15
IUE
FLUX
NUMBERS
X 10³
NGC 7009
C III]
1905
1907
1909
WAVELENGTH

FIG. 3

Figure Captions

Figure 1.
Low resolution spectra of the planetary nebulae NGC 6572 and IC 2165, taken through the large aperture with the SWP camera. The C III] feature at 1908 A is saturated in NGC 6572.

Figure 2.
Low resolution spectra of the planetary nebulae NGC 6572 and IC 2165, taken through the large aperature with the LWR camera. The small "x" 's indicate that the feature at 2200 A in both spectra is not real but results from a permanent "hot spot" on the detector surface.

Figure 3.
The C III] doublet near 1908 A in the high dispersion SWP spectrum of NGC 7009. The feature blueward of the 1906 line is not real but is an edge-of-order effect.